Paper Number: **106**

Title: **A Continuum Damage Mechanics Model to Predict Kink-Band Propagation Using Deformation Gradient Tensor Decomposition**

Authors: Andrew C. Bergan
Frank A. Leone Jr.

ABSTRACT

A new model is proposed that represents the kinematics of kink-band formation and propagation within the framework of a mesoscale continuum damage mechanics (CDM) model. The model uses the recently proposed deformation gradient decomposition approach to represent a kink band as a displacement jump via a cohesive interface that is embedded in an elastic bulk material. The model is capable of representing the combination of matrix failure in the frame of a misaligned fiber and instability due to shear nonlinearity. In contrast to conventional linear or bilinear strain softening laws used in most mesoscale CDM models for longitudinal compression, the constitutive response of the proposed model includes features predicted by detailed micromechanical models. These features include: 1) the rotational kinematics of the kink band, 2) an instability when the peak load is reached, and 3) a nonzero plateau stress under large strains.

INTRODUCTION

Composite plies in laminates loaded under longitudinal compression often fail by the kink-band damage mechanism [1]–[4]. A typical kink band is shown in Figure 1 along with the parameters often used to describe the kink band: w_{KB} for the width of the kink band, φ for the fiber misalignment angle, and β for the kink-band inclination angle. While failure criteria [5]–[9] and micromechanical models [10]–[14] have been developed with special consideration for the kinematics of kink bands, the majority of corresponding mesoscale damage propagation models utilize phenomenological softening laws that mirror the approach used for longitudinal tensile damage propagation [15]–[18]. Evaluations have shown that these existing phenomenological models that rely on linear or bilinear softening laws do not predict compressive failures accurately [19].

Andrew C Bergan, Structural Mechanics and Concepts Branch, NASA Langley Research Center, Mail Stop 190, Hampton, VA 23681, U.S.A.
Frank A. Leone, Jr., Structural Mechanics and Concepts Branch, NASA Langley Research Center, Mail Stop 190, Hampton, VA 23681, U.S.A.

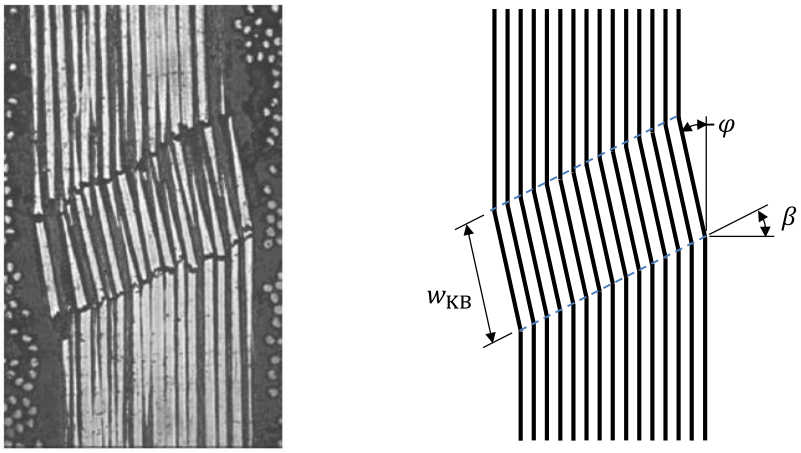

(a) Photomicrograph of a kink band [15]

(b) Conventional representation of a kink band

Figure 1. Kink band.

Many authors have contributed theoretical models that describe the formation of kink bands [20]. Argon [21] proposed that an initial fiber misalignment introduces shear stresses, which rotate fibers, further increasing shear stresses until failure is reached. Several authors subsequently recognized the importance of shear nonlinearity to the prediction of kink bands, e.g., [22]–[25]. The Langley Research Center (LaRC) failure criteria added the notions of 1) evaluating a matrix failure criterion in the misaligned fiber direction and 2) consideration of the competition between matrix cracking and instability due to shear nonlinearity for the prediction of strength [5], [6].

Two authors have proposed mesoscale models that include the post peak response. Basu et al. introduced a model that used Schapery Theory and stress transformations and showed the importance of considering multi-axial stress states [26]. Costa et al. recently extended these concepts to account for the post-peak response considering matrix damage, shear nonlinearity, and friction while also addressing the need for special considerations to achieve mesh objectivity [27].

The purpose of this paper is to propose a mesoscale continuum damage mechanics (CDM) model for longitudinal compression based on the assumptions of the LaRC failure criteria. The deformation gradient decomposition (DGD) method [28] is used for accurate representation of the kink band and fiber misalignments.

MODEL OVERVIEW

The model formulation and implementation are described in this section. It is assumed that the kink-band plane occurs in the 1-2 plane to simplify the derivation. The model formulation can be extended to consider out-of-plane kinking by adding a criterion for the kinking plane angle as described in LaRC04 [6].

Idealization of the Kink-Band Formation Process

The idealization of the kink-band formation process builds on Argon's hypothesis that an initial fiber misalignment leads to fiber rotation and increasing shear stress in the matrix, eventually initiating matrix failure. Recent, detailed experimental investigations have revealed that Mode II microcracks form between the fibers during kink band formation, e.g., [29]. The formation of matrix cracks as a result of fiber rotation is consistent with the LaRC03 model proposed by Dávila and Camanho [5], which builds on Argon's model by evaluating a matrix failure criterion in the coordinate frame of the rotated (misaligned) fibers. Pinho et al. [6] extended this concept in the LaRC04 model by adding shear-nonlinearity. Additionally, Pinho et al. proposed that kink bands initiate due to one of two competing failure mechanisms: 1) matrix failure or 2) instability due to shear nonlinearity. The model proposed here accounts for the initiation and evolution of both of these mechanisms (matrix failure and instability due to shear nonlinearity) within the framework of a mesoscale CDM. The model collapses matrix cracks on a single cohesive interface that is embedded within a bulk material, as shown in Figure 2. Furthermore, the model assumes that bending of the fibers and the kink-band inclination angle can be ignored, as presumed by the idealization shown in Figure 2. The bulk material is represented with a constitutive model that includes shear nonlinearity.

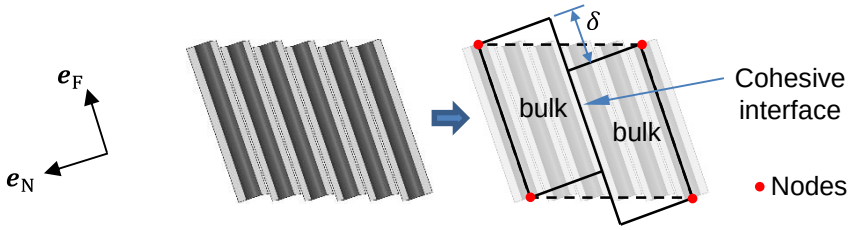

Figure 2. Splitting microcracks in-between fibers are lumped into a cohesive interface that is embedded within a bulk material.

The sequence of the material behavior under increasing longitudinal load is shown schematically in Figure 3. In the undeformed condition, Figure 3a, an initial fiber misalignment, φ_0, is assumed to represent the presence of defects that affect the longitudinal compressive strength. As longitudinal compression loading is introduced, rotation due to anisotropy occurs so that the current fiber misalignment is a function of φ_0 and the shear strain, γ_{FN}, as shown in Figure 3b. Following Pinho's hypothesis, the strength is reached when either of the two competing failure mechanisms occur: 1) instability due to shear nonlinearity or 2) failure in the matrix. Even if instability due to shear nonlinearity occurs first, under increasing load, a crack will eventually initiate along the embedded cohesive interface, as shown in Figure 3c. Once the crack initiates, an unstable positive feedback loop develops where softening along the cohesive interface allows larger fiber rotation, which in turn drives further damage of the cohesive interface. Eventually, φ becomes large enough that compressive stress in the crack-normal direction and friction arrest the instability.

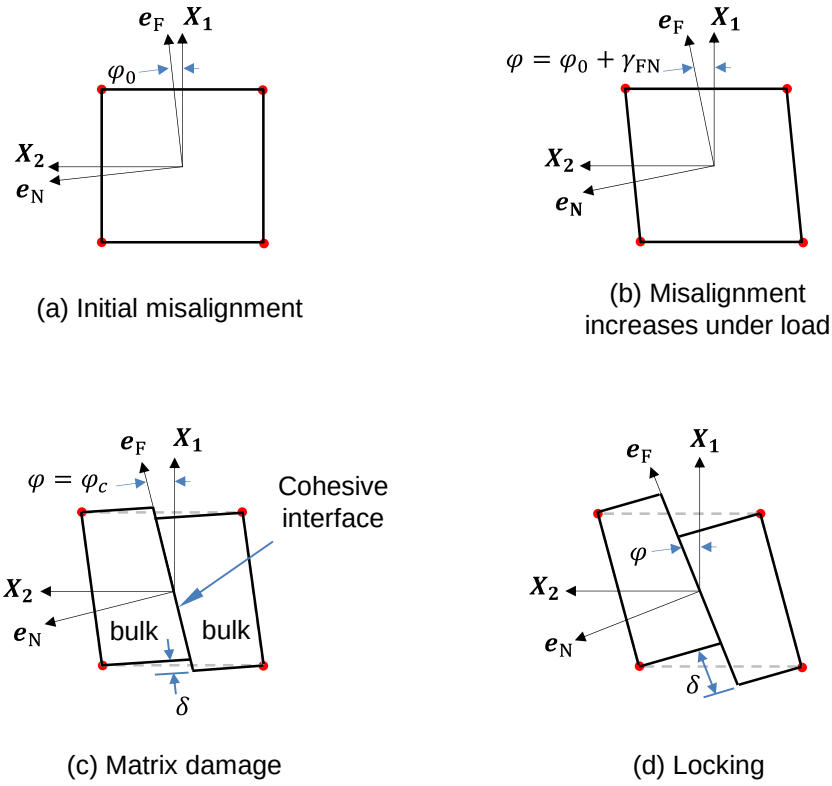

Figure 3. Schematic representation of the kink band model kinematics.

DGD-Based Formulation

The kinematics of kink band formation illustrated in Figure 3 can be modeled using a formulation based on the DGD approach [28]. Consider a rectangular continuum of fiber-reinforced material where the fiber direction is initially aligned with the reference X_1-direction. The reference configuration is defined as

$$\boldsymbol{X} = \begin{bmatrix} l_1 & 0 & 0 \\ 0 & l_2 & 0 \\ 0 & 0 & l_3 \end{bmatrix} \tag{1}$$

where the nonzero diagonal components are the undeformed dimensions of the continuum. The current configuration, $\boldsymbol{x}$, is a function of $\boldsymbol{X}$ and the deformation gradient tensor, $\boldsymbol{F}$

$$\boldsymbol{x} = \boldsymbol{F}\boldsymbol{X} \tag{2}$$

The deformation gradient tensor, $\boldsymbol{F}$, maps the coordinates defined in the reference configuration to their relative locations in the current configuration. The objective of the material model formulated in this section is to determine the stress in the continuum knowing the deformation state $\boldsymbol{F}$.

DEFORMATION GRADIENT DECOMPOSITION

A kink band may develop in the continuum having a width, w_{kb}, that is a function of the material properties and stress state. Therefore, w_{kb} is independent of the continuum dimension in the longitudinal direction, l_1. Herein, it is assumed that $w_{\text{kb}} \leq$

l_1. As a result of this assumption, the continuum is decomposed into the kink-band region and the neighboring undamaged material region, as shown in Figure 4a. The kink-band region is further subdivided into a cohesive interface and a bulk region following the idealization introduced in Figure 2. The three regions and their corresponding deformation measures shown in Figure 4b are identified: 1) the cohesive interface, $\boldsymbol{\delta}$; 2) the kink-band bulk material, $\boldsymbol{F}_{\mathrm{B}}$; and 3) the undamaged material region, $\boldsymbol{F}_{\mathrm{M}}$. The deformation of the kink-band region is $\boldsymbol{F}_{\mathrm{KB}}$, which includes the deformation of $\boldsymbol{\delta}$ and $\boldsymbol{F}_{\mathrm{B}}$. While the cohesive interface is illustrated in the center of the kink-band region, location of the interface is arbitrary within the kink-band region. Leone's DGD methodology [28] is used to decompose the continuum deformation state $\boldsymbol{F}$ into $\boldsymbol{\delta}$, $\boldsymbol{F}_{\mathrm{B}}$, and $\boldsymbol{F}_{\mathrm{M}}$ as described in the following.

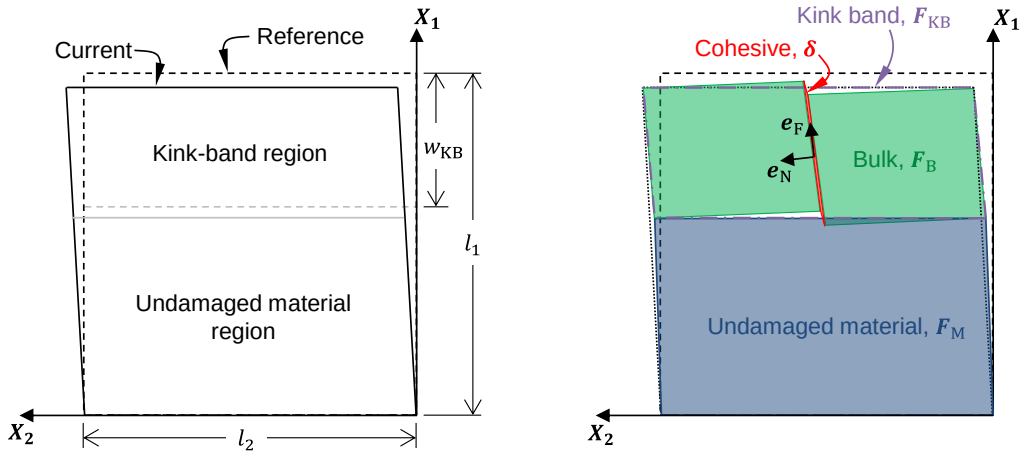

(a) Decomposition into kink-band and undamaged material regions

(b) Model regions and deformations

Figure 4. Schematic representation of the model.

In the undeformed configuration, the fibers are misaligned by the angle φ_0. When the continuum is deformed under compressive loads, the fiber direction rotates as a result of the anisotropy from the initial misalignment. Since it is assumed that matrix damage may develop and propagate along the fiber direction, it is necessary to track the cohesive interface, which is aligned with the fiber direction. A coordinate system $\boldsymbol{R}_{\mathbf{cr}}$ can be defined to track the cohesive interface orientation:

$$\boldsymbol{R}_{\mathrm{cr}} = [\hat{\boldsymbol{e}}_{\mathrm{F}} \quad \hat{\boldsymbol{e}}_{\mathrm{N}} \quad \hat{\boldsymbol{e}}_{\mathrm{T}}] \tag{3}$$

where the unit vectors are defined as

$$\boldsymbol{e}_{\mathrm{F}} = \boldsymbol{F}_{\mathrm{B}} \begin{bmatrix} \cos\varphi_0 \\ \sin\varphi_0 \\ 0 \end{bmatrix} \tag{4}$$

$$\boldsymbol{e}_{\mathrm{N}} = \boldsymbol{F}_{\mathrm{B}}^{-\mathrm{T}} \begin{bmatrix} -\sin\varphi_0 \\ \cos\varphi_0 \\ 0 \end{bmatrix} \tag{5}$$

$$\boldsymbol{e}_{\mathrm{T}} = \boldsymbol{e}_{\mathrm{F}} \times \boldsymbol{e}_{\mathrm{N}} \tag{6}$$

Compatibility considerations are invoked to determine expressions for $\boldsymbol{\delta}$, $\boldsymbol{F}_{\mathrm{B}}$, $\boldsymbol{F}_{\mathrm{KB}}$, and $\boldsymbol{F}_{\mathrm{M}}$. First, $\boldsymbol{F}$ is decomposed into $\boldsymbol{F}_{\mathrm{M}}$ and $\boldsymbol{F}_{\mathrm{KB}}$ as shown in Figure 5a. In the fiber direction, compatibility of the deformations requires

$$\boldsymbol{x}^{(1)} = (1 - \omega_{\mathrm{KB}})\boldsymbol{x}_{\mathrm{M}}^{(1)} + \omega_{\mathrm{KB}}\boldsymbol{x}_{\mathrm{KB}}^{(1)} \tag{7}$$

where the superscript $^{(1)}$ indicates the first column of $\boldsymbol{x}$ and ω_{KB} is the normalized width of the kink band, $\omega_{\mathrm{KB}} = w_{\mathrm{KB}}/l_1$. Substituting equations (2) and (1) into equation (7)

$$\boldsymbol{F}\boldsymbol{X}^{(1)} = (1 - \omega_{\mathrm{KB}})\boldsymbol{F}_{\mathrm{M}}\boldsymbol{X}^{(1)} + \omega_{\mathrm{KB}}\boldsymbol{F}_{\mathrm{KB}}\boldsymbol{X}^{(1)} \tag{8}$$

then simplifying and rearranging yields an expression for $\boldsymbol{F}_{\mathrm{KB}}^{(1)}$:

$$\boldsymbol{F}_{\mathrm{KB}}^{(1)} = \frac{1}{\omega_{\mathrm{KB}}}\boldsymbol{F}^{(1)} + \left(1 - \frac{1}{\omega_{\mathrm{KB}}}\right)\boldsymbol{F}_{\mathrm{M}}^{(1)} \tag{9}$$

In the 2-direction, there is no decomposition, so compatibility of the deformation requires

$$\boldsymbol{x}_{\mathrm{KB}}^{(2)} = \boldsymbol{x}_{\mathrm{M}}^{(2)} = \boldsymbol{x}^{(2)} \tag{10}$$

Substituting equation (2) into (10) and simplifying yields

$$\boldsymbol{F}_{\mathrm{KB}}^{(2)} = \boldsymbol{F}_{\mathrm{M}}^{(2)} = \boldsymbol{F}^{(2)} \tag{11}$$

Similarly, $\boldsymbol{F}_{\mathrm{KB}}$ is decomposed into $\boldsymbol{\delta}$ and $\boldsymbol{F}_{\mathrm{B}}$ as shown in Figure 5b. Again, compatibility considerations introduce relationships in the fiber direction and in the transverse directions. In the fiber direction,

$$\boldsymbol{F}_{\mathrm{B}}^{(1)} = \boldsymbol{F}_{\mathrm{KB}}^{(1)} \tag{12}$$

In the crack-normal direction,

$$\boldsymbol{x}_{\mathrm{KB}}^{(2)} = \boldsymbol{x}_{\mathrm{B}}^{(2)} + \boldsymbol{R}_{\mathrm{cr}}\boldsymbol{\delta} \tag{13}$$

Substituting equation (2) into (13)

$$\boldsymbol{F}_{\mathrm{KB}}\boldsymbol{X}^{(2)} = \boldsymbol{F}_{\mathrm{B}}\boldsymbol{X}^{(2)} + \boldsymbol{R}_{\mathrm{cr}}\boldsymbol{\delta} \tag{14}$$

and rearranging yields

$$\boldsymbol{\delta} = \boldsymbol{R}_{\mathrm{cr}}^{\mathrm{T}}\left(\boldsymbol{F}_{\mathrm{B}}^{(2)} - \boldsymbol{F}^{(2)}\right)l_2 \tag{15}$$

Using equations (9) – (11), (12), and (15) with $\boldsymbol{F}$ provided as an input, the quantities $\boldsymbol{\delta}$, $\boldsymbol{F}_{\mathrm{B}}$, $\boldsymbol{F}_{\mathrm{KB}}$, and $\boldsymbol{F}_{\mathrm{M}}$ can be determined in terms of $\boldsymbol{F}_{\mathrm{B}}^{(2)}$ and $\boldsymbol{F}_{\mathrm{M}}^{(1)}$.

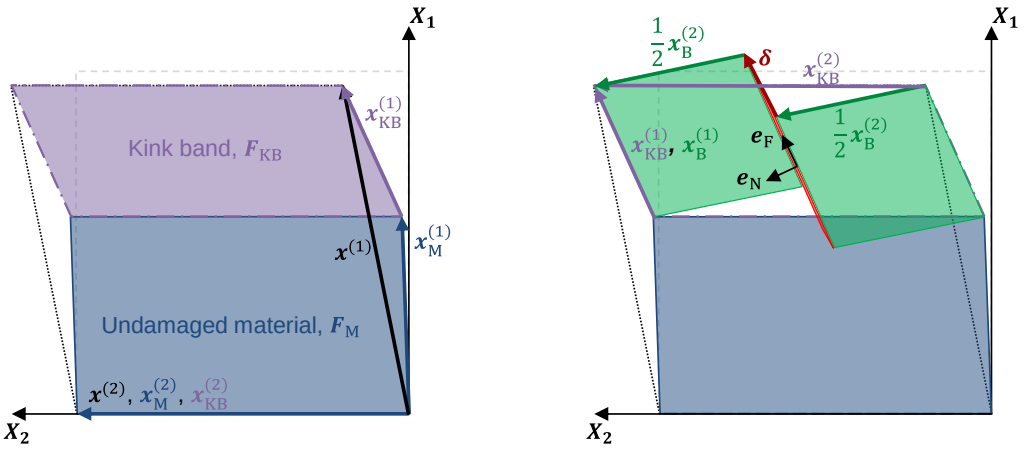

(a) Decomposition of $\boldsymbol{F}$ into $\boldsymbol{F}_{\mathrm{KB}}$ and $\boldsymbol{F}_{\mathrm{M}}$

(b) Decomposition of $\boldsymbol{F}_{\mathrm{KB}}$ into $\boldsymbol{F}_B$ and $\boldsymbol{\delta}$

Figure 5. Decomposition of the continuum.

EQUILIBRIUM AND SOLUTION PROCEDURE

It is necessary to ensure that the tractions that arise in the cohesive interface, kink-band bulk, and neighboring material are in equilibrium. Equilibrium is enforced 1) between the cohesive interface and the kink-band bulk material in the crack-normal direction, $\hat{\boldsymbol{e}}_{\mathrm{N}}$ and 2) between the kink-band region and the neighboring material in the fiber direction, $\hat{\boldsymbol{e}}_{\mathrm{F}}$.

First, the tractions on the cohesive interface are derived as follows. The cohesive stress vector $\boldsymbol{\tau}_{\mathrm{COH}}$ is determined using the cohesive damage model proposed by Turon et al. [30]. The cohesive stress vector $\boldsymbol{\tau}_{\mathrm{COH}}$ is defined as

$$\boldsymbol{\tau}_{\mathrm{COH}} = \begin{bmatrix} k_{\mathrm{F}}(1-d_m)\delta_{\mathrm{F}} \\ k_{\mathrm{N}}(1-d_m)\delta_{\mathrm{N}} - k_{\mathrm{N}}d_m\langle-\delta_{\mathrm{N}}\rangle \\ k_{\mathrm{T}}(1-d_m)\delta_{\mathrm{T}} \end{bmatrix} \tag{16}$$

where δ_{F}, δ_{N}, and δ_{T} are the components of $\boldsymbol{\delta}$ along the fiber, crack-normal, and transverse directions, respectively; k_{F}, k_{N}, and k_{T} are the cohesive penalty stiffnesses in the fiber, crack-normal, and transverse directions, respectively; d_m is the scalar cohesive damage variable; and the operator $\langle x\rangle$ is defined as $\langle x\rangle = (x + |x|)/2$. The stress in the kink-band bulk is determined from $\boldsymbol{F}_{\mathrm{B}}$ using Green-Lagrange strain and Hooke's Law as

$$\boldsymbol{E}_{\mathrm{B}} = \frac{1}{2}\left(\boldsymbol{F}_{\mathrm{B}}^{\mathrm{T}}\boldsymbol{F}_{\mathrm{B}} - \boldsymbol{I}\right) - \frac{\gamma_{\mathrm{PL}}}{2}\begin{bmatrix} 0 & 1 & 0 \\ 1 & 0 & 0 \\ 0 & 0 & 0 \end{bmatrix} \tag{17}$$

$$\boldsymbol{S}_{\mathrm{B}} = \boldsymbol{C}_{\varphi_0} : \boldsymbol{E}_{\mathrm{B}} \tag{18}$$

where $\boldsymbol{E}_{\mathrm{B}}$ is the Green-Lagrange strain, $\boldsymbol{I}$ is the identity tensor, $\boldsymbol{S}_{\mathrm{B}}$ is the 2nd Piola-Kirchhoff stress, $\boldsymbol{C}_{\varphi_0}$ is the stiffness tensor rotated about the transverse direction by φ_0 following classical lamination theory (see, e.g., [31]), and γ_{PL} is the plastic portion of the shear strain ($\gamma = \gamma_{\mathrm{EL}} + \gamma_{\mathrm{PL}}$). A variation of the Ramberg-Osgood model [32]

$$\gamma_{12} = \frac{1}{G_{12}}\left[\tau_{12} + \alpha_{\mathrm{PL}}\mathrm{sign}(\tau_{12})|\tau_{12}|^{n_{\mathrm{PL}}}\right] \tag{19}$$

is used to represent shear-nonlinearity in the bulk material. The plastic portion of the shear strain γ_{PL} is found through iteration and is removed from the strain tensor as shown in equation (17). By transforming $\boldsymbol{S}_{\mathrm{B}}$ to Cauchy stress as

$$\boldsymbol{\sigma}_{\mathrm{B}} = \boldsymbol{F}_{\mathrm{B}}\boldsymbol{S}_{\mathrm{B}}\boldsymbol{F}_{\mathrm{B}}^{\mathrm{T}}|\boldsymbol{F}_{\mathrm{B}}|^{-1} \tag{20}$$

Cauchy's stress theorem can be used to find the stress vector acting on the cohesive interface:

$$\boldsymbol{t}_{\mathrm{B}} = \boldsymbol{\sigma}_{\mathrm{B}} \cdot \hat{\boldsymbol{e}}_{\mathrm{N}} \tag{21}$$

Likewise, the tractions for equilibrium between the kink-band region and the neighboring material in the fiber direction are derived as follows. In the neighboring material, the Cauchy stress is

$$\boldsymbol{\sigma}_{\mathrm{M}} = \boldsymbol{F}_{\mathrm{M}}\boldsymbol{S}_{\mathrm{M}}\boldsymbol{F}_{\mathrm{M}}^{\mathrm{T}}|\boldsymbol{F}_{\mathrm{M}}|^{-1} \tag{22}$$

where

$$\boldsymbol{S}_{\mathrm{M}} = \boldsymbol{C}_{\varphi_0} : \boldsymbol{E}_{\mathrm{M}} \tag{23}$$

$$\boldsymbol{E}_{\mathrm{M}} = \frac{1}{2}\left(\boldsymbol{F}_{\mathrm{M}}^{\mathrm{T}}\boldsymbol{F}_{\mathrm{M}} - \boldsymbol{I}\right) - \frac{\gamma_{\mathrm{PL}}}{2}\begin{bmatrix} 0 & 1 & 0 \\ 1 & 0 & 0 \\ 0 & 0 & 0 \end{bmatrix} \tag{24}$$

Cauchy's stress theorem is used to obtain the stress vector acting on a plane defined by the fiber direction in the kink-band:

$$\boldsymbol{t}_{\mathrm{M}} = \boldsymbol{\sigma}_{\mathrm{M}} \cdot \hat{\boldsymbol{e}}_{\boldsymbol{F}} \tag{25}$$

The corresponding traction due to the stress in the kink-band region is

$$\boldsymbol{t}_{\mathrm{KB}} = \boldsymbol{\sigma}_{\mathrm{B}} \cdot \hat{\boldsymbol{e}}_{\boldsymbol{F}} \tag{26}$$

An iterative solution procedure is required to solve for the state of stress at equilibrium. A residual stress vector $\boldsymbol{\sigma}_{\mathrm{res}}$ is defined in terms of the stress vectors in equations (16), (21), (25), and (26) in the current crack coordinate system as

$$\boldsymbol{\sigma}_{\mathrm{res}} = \begin{bmatrix} \boldsymbol{R}_{\mathrm{cr}}^{\mathrm{T}}(\boldsymbol{t}_{\mathrm{M}} - \boldsymbol{t}_{\mathrm{KB}}) \\ \boldsymbol{\tau}_{\mathrm{COH}} - \boldsymbol{R}_{\mathrm{cr}}^{\mathrm{T}}\boldsymbol{t}_{\mathrm{B}} \end{bmatrix} \tag{27}$$

where the unknown variables are

$$\boldsymbol{x}_{\mathrm{eq}} = \begin{bmatrix} \boldsymbol{F}_{\mathrm{M}}^{(1)} \\ \boldsymbol{F}_{\mathrm{B}}^{(2)} \end{bmatrix} \tag{28}$$

The Newton-Raphson method is used following

$$\boldsymbol{x}_{\mathrm{eq,new}} = \boldsymbol{x}_{\mathrm{eq}} - \left(\frac{\partial \boldsymbol{\sigma}_{\mathrm{res}}}{\partial \boldsymbol{x}_{\mathrm{eq}}}\right)^{-1} \boldsymbol{\sigma}_{\mathrm{res}} \tag{29}$$

to find a converged solution for $\boldsymbol{x}_{\mathrm{eq}}$ by iterating until the norm of $\boldsymbol{\sigma}_{\mathrm{res}}$ is less than a tolerance value (in this case, set to 0.01% of the Mode I cohesive strength). After the converged solution is found, the cohesive damage model is evaluated to determine d_m for the current $\boldsymbol{\delta}$. If d_m increases, a new converged deformation state is sought for the updated d_m using equation (29). If d_m does not increase, a solution for the current $\boldsymbol{F}$ has been found and the stress in the kink-band bulk material is returned.

FRICTION ACTING ON THE CRACK

Compressive failures, whether matrix or fiber dominated, often propagate unstably. Friction on the fracture surfaces can stabilize these failure processes. As a result, accounting for friction on compressively loaded cracks can have a significant effect on the structural response.

In order to predict matrix cracking while under compressive loading, it is important to account for the effects of friction on the potential fracture planes. Prior to failure initiation, compressive stresses on a fracture plane are known to increase the effective shear strength (e.g., [6], [33]). Camanho et al. [17] accounted for this increased effective shear strength for matrix cracks in his smeared crack continuum damage mechanics model. In the present model, the approach of Camanho et al. is used to predict the σ_{12} vs. σ_{22} failure initiation envelope of LaRC04.

In order to account for the effects of friction on the matrix cracks after initiation, features of the cohesive zone model of Alfano and Sacco [34] were applied. In the Alfano-Sacco model, friction acts only on the damaged portion of a cohesive zone element, which causes the surface area on which friction acts to increase as the cohesive damage variable increases. A single, constant coefficient of friction is assumed.

DEMONSTRATION AND DISCUSSION

The proposed model is demonstrated in this section. The model was implemented as VUMAT in Abaqus [35]. Several features of the model are highlighted in this section through single element analyses. The contributions of the initial misalignment angle, the cohesive interface fracture toughness, and the coefficient of friction to the constitutive response of the model are investigated. The material properties for IM7-8552 used in this section are summarized in Table I. The width of the kink band was assumed to be 0.1 mm. A single element (C3D8R) model was used with uniform end shortening displacement applied to the longitudinal direction. The element size was 0.15 mm on all sides. The applied displacement was reacted by simply supported boundary conditions on the opposite face.

TABLE I. IM7-8552 MATERIAL PROPERTIES.

Property	Value	Units	Source
E_{11}	171420	MPa	[36]
E_{22}	9080	MPa	[36]
G_{12}	5290	MPa	[36]
ν_{12}	0.32	-	[36]
ν_{23}	0.52	-	[17]
α_{PL}	4.41×10^{-10}	$\mathrm{MPa}^{1-\eta_{\mathrm{PL}}}$	[37]
n_{PL}	5.934	-	[37]
X_C	1200	MPa	[17]
Y_C	199.8	MPa	[36]
S_L	92.3	MPa	[36]
Y_T	62.3	MPa	[36]
G_{Ic}	0.277	N/mm	[17]
G_{IIc}	0.788	N/mm	[17]
η_{BK}	1.634	-	[17]
μ	0.3	-	Assumed

Initial Misalignment Angle

As with many failure criteria for longitudinal compression failure, the present model assumes an initial fiber misalignment angle φ_0. The effect of φ_0 is illustrated in Figure 6 for a range of values where the longitudinal stress ($\sigma_{11} = RF1/A$) normalized to the strength is plotted as a function of applied longitudinal strain. The analyses were terminated when the matrix failure criterion was satisfied on the cohesive interface, which occurred in all cases.

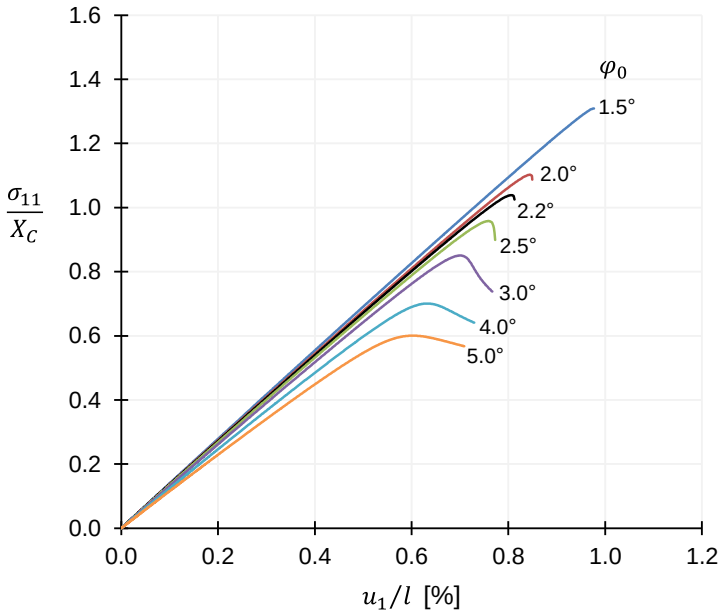

Figure 6. Effect of φ_0 on the predicted response. Results are truncated at the point when matrix failure initiates.

Pinho et al. [6] and Camanho et al. [9] proposed procedures to determine the φ_0 that corresponds to a measured strength X_C taking into account shear nonlinearity. In both cases, φ_0 is obtained from

$$\varphi_0 = \varphi_c - \gamma_{FN} \tag{30}$$

where φ_c is the rotation of the fibers when the strength X_C is reached for a uniaxial stress state. The values of φ_0 calculated following Pinho et al. [6] and Camanho et al. [9] for the material properties in Table I are similar: 3.5° and 3.4°, respectively. For both these values of φ_0, the present model underpredicts the strength significantly, as shown in Figure 6. Also, in both cases, the present model predicts that instability due to shear nonlinearity occurs before matrix failure, as can be observed in Figure 6 by the gradual unloading after the peak load prior to failure initiation in the matrix.

A graphical comparison of the shear nonlinearity stress-strain curve based on equation (19), and the applied shear stress provides insight into the transition between instability due to shear nonlinearity and matrix failure, as proposed in [6]. For uniaxial compressive loading with $\sigma_{11} = X_C$, the shear stress in the misaligned frame can be obtained from a stress transformation by the angle $\varphi = \varphi_0 + \gamma$:

$$\tau = \frac{1}{2}\sin\big(2(\varphi_0 + \gamma)\big)\, X_C \tag{31}$$

The graphical comparison of equations (19) and (31) for the material properties considered here is shown in Figure 7. Equation (31) is plotted in Figure 7 with several values for φ_0. According to [6], matrix failure occurs prior to instability for values of φ_0 that intersect the shear stress-strain curve (i.e., $\varphi_0 = 1.5°$ in Figure 7), and failure occurs by instability when equation (31) does not intersect with the shear stress-strain curve (e.g. $\varphi_0 > 2.2°$). Such is the case here for the values of $\varphi_0 = 3.5°$ or 3.4° calculated using equation (30). Therefore, a different criterion is required to determine φ_0 in the case of shear instability.

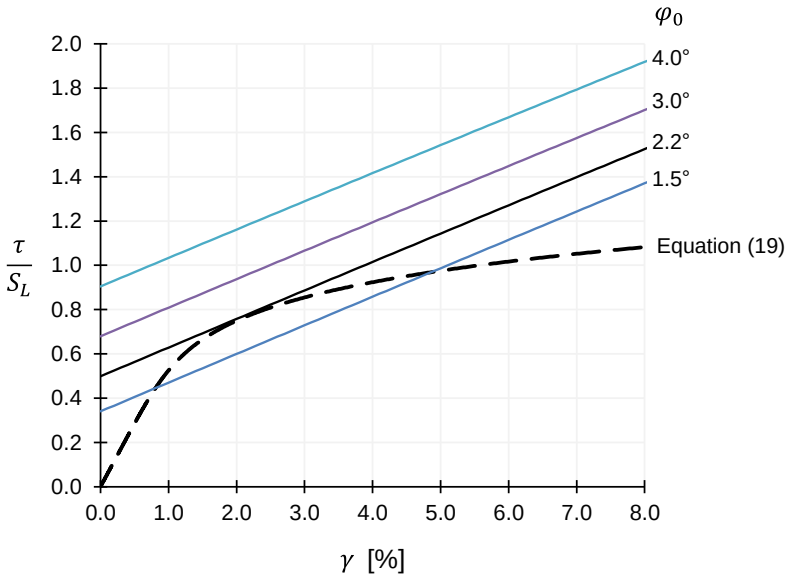

Figure 7. Criterion for matrix failure vs. instability due to shear nonlinearity, where the transition between modes occurs for the φ_0 that makes the results from equation (31) tangent to equation (19), after [6].

Pinho et al. [6] suggested that when failure occurs by instability, φ_0 can be found by requiring that the result from equation (31) is tangent to the result from equation (19). For the material properties in Table I, the tangency criterion produces $\varphi_0 = 2.2°$. It is observed that when $\varphi_0 = 2.2°$ is used in the present model, the strength is reproduced accurately (3.9% error) as shown in Figure 6. Therefore, $\varphi_0 = 2.2°$ is used in the analyses described in subsequent sections.

The results shown in Figure 6 indicate that the initial misalignment angle φ_0 has an effect on the compression modulus. The initial misalignment angle yields a good approximation of a compressive elastic modulus even though a tensile elastic modulus is used as the material property input. The elastic stiffness produced by the model is $E_{11,C} = 159{,}180$ MPa, which compares well with the value of 149,600 MPa found in [38]. Therefore, the use of an initial misalignment angle yields a good approximation of the reduction in the Young's modulus from tension to compression.

Constitutive Response

The constitutive response of the model under unidirectional compression using the nominal material properties in Table I is shown in Figure 8. Several important features of the constitutive response include 1) pre-peak nonlinearity, 2) large fiber rotation immediately following the peak stress, and 3) a non-zero plateau stress at large strains. The trend of the constitutive response is consistent with responses predicted by detailed micromechanical models, e.g., [10], [11], which is to say a significant departure from commonly used linear or bilinear softening laws.

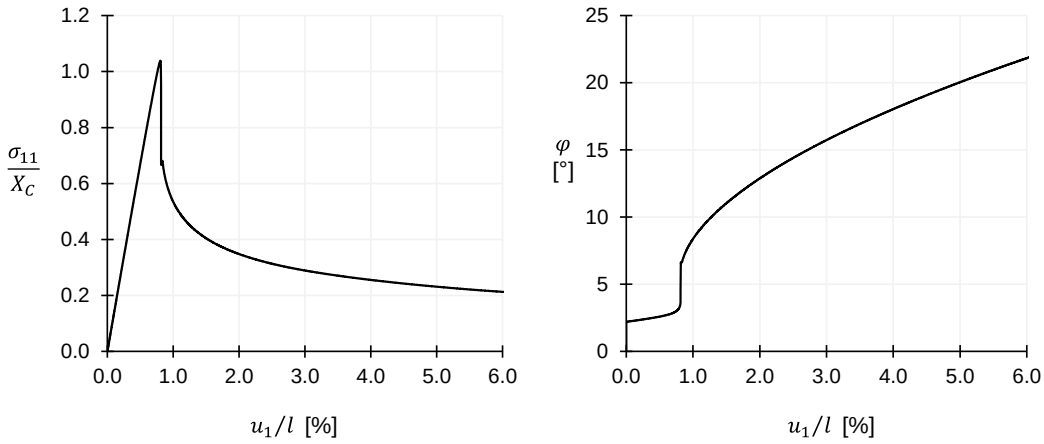

Figure 8. Constitutive response of the model for uniaxial compressive loading.

The fact that the model includes the rotation in the kink-band is of particular importance. Experimental observations of kink-bands often show that the rotation of the kinkband leads to an interaction with matrix cracks and delaminations in the adjacent plies [4], [19]. Since this model includes the rotation of the kink band, it shows promise for reproducing the interactions between kink-bands, delaminations, and matrix cracks when applied in a structural analysis.

Effect of Mode II Fracture Toughness and Friction

The matrix crack represented by the cohesive interface exhibits sliding with $\tau_N < 0$ and so the Mode II fracture toughness, G_{IIc}, and the coefficient of friction, μ, may play important roles in the constitutive response of the model.

The constitutive responses of the model for three values of G_{IIc} (G_{IIc}, $0.5G_{IIc}$, and $10G_{IIc}$) are shown in Figure 9. In order to isolate the influence of G_{IIc} from frictional effects, the results shown are for $\mu = 0$. When small values for G_{IIc} are used, the instability and vibration becomes more severe. The model shows comparatively less sensitivity to larges values of G_{IIc}. In general, it is observed that G_{IIc} influences the steady-state plateau stress.

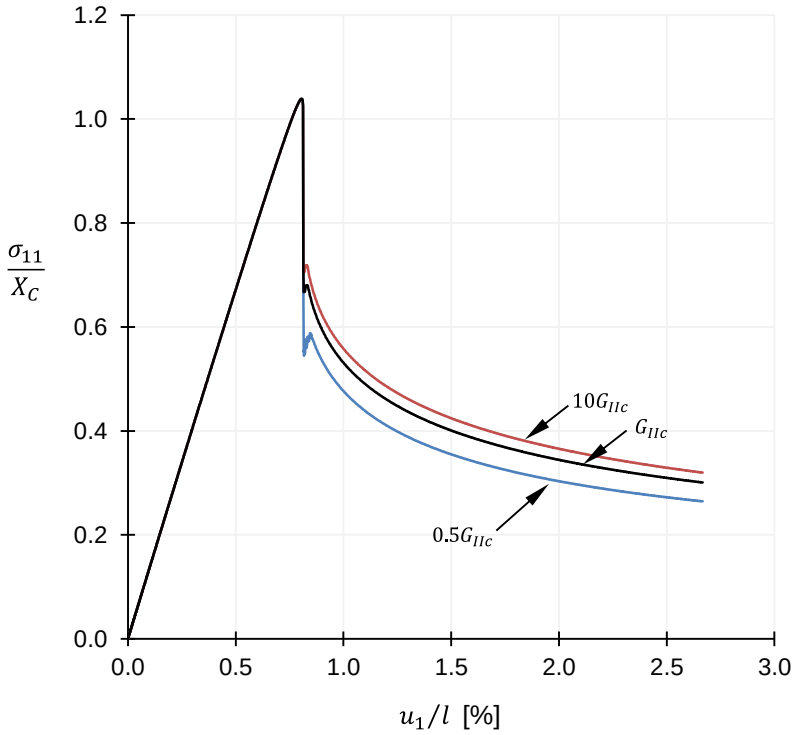

Figure 9. Effect of fracture toughness.

The coefficient of friction, μ, used on the cohesive interface was varied to investigate the sensitivity of the model to this parameter. No experimentally determined value of μ was available. The longitudinal responses for three values of μ are shown in Figure 10. The results indicate that the model is relatively insensitive to μ. Therefore, the assumed value has little bearing on the response characteristics and may not be important for structural predictions for materials such as IM7-8552 that fail by shear instability.

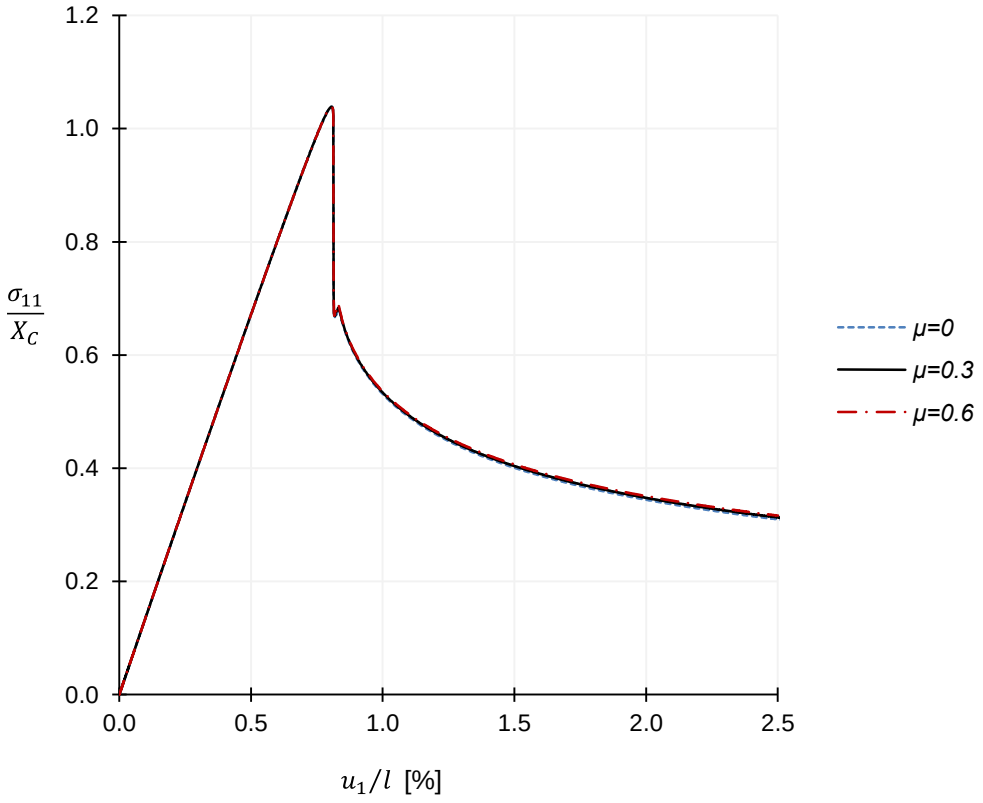

Figure 10. Effect of the coefficient of friction.

SUMMARY

A new mesoscale continuum damage mechanics (CDM) model has been proposed to represent the constitutive response of plies subjected to longitudinal compression loading. The model is formulated on the basis of the assumptions proposed in the LaRC failure criteria and uses the deformation gradient decomposition approach to track the rotation of the fibers through loading. The model is capable of representing several features in the constitutive response, including the compressive stiffness, the strength, the potential instability at kink-band onset, and the post-peak plateau stress. These response characteristics agree with the trends predicted by detailed micromechanical analyses. Since this model includes the rotation of the kink band, it shows promise for reproducing the interactions between kink-bands, delaminations, and matrix cracks when applied in a structural analysis.

REFERENCES

[1] Suemasu, H., Y. Naito, K. Gozu, and Y. Aoki. 2012. "Damage Initiation and Growth in Composite Laminates during Open Hole Compression Tests," *Adv. Compos. Mater.*, 21(3):209-220.

[2] Hapke, J., F. Gehrig, N. Huber, K. Schulte, and E. T. Lilleodden. 2011. "Compressive Failure of UD-CFRP Containing Void Defects: In Situ SEM Microanalysis," *Compos. Sci. Technol.*, 71(9):1242-1249.

[3] Gutkin, R. and S. T. Pinho. 2015. "Combining Damage and Friction to Model Compressive Damage Growth in Fibre-Reinforced Composites," *J. Compos. Mater.*, 49(20):2483–2495.

[4] Zobeiry, N., R. Vaziri, and A. Poursartip. 2015. "Characterization of Strain-Softening Behavior and Failure Mechanisms of Composites under Tension and Compression," *Compos. Part Appl. Sci. Manuf.*, 68:29–41.
[5] Dávila, C. G. and P. P. Camanho. 2003. "Failure Criteria for FRP Laminates in Plane Stress," NASA/TM-2003-212663, NASA Langley Research Center.
[6] Pinho, S. T., C. G. Dávila, P. P. Camanho, L. Iannucci, and P. Robinson. 2005. "Failure Models and Criteria for FRP under In-Plane or Three-Dimensional Stress States Including Shear Non-Linearity," NASA/TM-2005-213530, NASA Langley Research Center.
[7] Gutkin, R., S. T. Pinho, P. Robinson, and P. T. Curtis, "A Finite Fracture Mechanics Formulation to Predict Fibre Kinking and Splitting in CFRP under Combined Longitudinal Compression and In-Plane Shear," *Mech. Mater.*, 43(11):730–739.
[8] Catalanotti, G., P. P. Camanho, and A. T. Marques. 2013. "Three-Dimensional Failure Criteria for Fiber-Reinforced Laminates," *Compos. Struct.*, 95:63–79.
[9] Camanho, P. P., A. Arteiro, A. R. Melro, G. Catalanotti, and M. Vogler. 2015. "Three-Dimensional Invariant-Based Failure Criteria for Fibre-Reinforced Composites," *Int. J. Solids Struct.*, 55:92–107.
[10] Pimenta, S., R. Gutkin, S. T. Pinho, and P. Robinson. 2009. "A Micromechanical Model for Kink-Band Formation: Part I — Experimental Study and Numerical Modelling," *Compos. Sci. Technol.*, 69(7–8):948–955.
[11] Pimenta, S., R. Gutkin, S. T. Pinho, and P. Robinson. 2009. "A Micromechanical Model for Kink-Band Formation: Part II—Analytical Modelling," *Compos. Sci. Technol.*, 69(7–8):956–964.
[12] Gutkin, R., S. T. Pinho, P. Robinson, and P. T. Curtis. 2010. "Micro-Mechanical Modelling of Shear-Driven Fibre Compressive Failure and of Fibre Kinking for Failure Envelope Generation in CFRP Laminates," *Compos. Sci. Technol.*, 70(8):1214–1222.
[13] Bai, X., M. A. Bessa, A. R. Melro, P. P. Camanho, L. Guo, and W. K. Liu. 2015. "High-Fidelity Micro-Scale Modeling of the Thermo-Visco-Plastic Behavior of Carbon Fiber Polymer Matrix Composites," *Compos. Struct.*, 134:132–141.
[14] Naya, F., C. González, C. S. Lopes, S. Van der Veen, and F. Pons. 2016. "Computational Micromechanics of the Longitudinal Behaviour of Unidirectional Fibre Reinforced Polymers Including Environmental Effects," *Compos. Sci. Technol.*, submitted.
[15] Maimí, P., P. P. Camanho, J.-A. Mayugo, and C. G. Dávila. 2006. "A Thermodynamically Consistent Damage Model for Advanced Composites," NASA/TM-2006-214282, NASA Langley Research Center.
[16] Pinho, S. T., L. Iannucci, and P. Robinson. 2006. "Physically Based Failure Models and Criteria for Laminated Fibre-Reinforced Composites with Emphasis on Fibre Kinking. Part II: FE Implementation," *Compos. Part Appl. Sci. Manuf.*, 37(5):766–777.
[17] Camanho, P. P., M. A. Bessa, G. Catalanotti, M. Vogler, and R. Rolfes. 2013. "Modeling the Inelastic Deformation and Fracture of Polymer Composites – Part II: Smeared Crack Model," *Mech. Mater.*, 59:36–49.
[18] Iarve, E. V., K. Hoos, M. Braginsky, E. Zhou, and D. H. Mollenhauer. 2015. "Tensile and Compressive Strength Prediction in Laminated Composites by Using Discrete Damage Modeling," presented at the AIAA/ASME/ASCE/AHS/ASC Structures, Structural Dynamics, and Materials Conference, January 5-9, 2015.
[19] Sola, C., B. Castanié, L. Michel, F. Lachaud, A. Delabie, and E. Mermoz. 2016. "On the Role of Kinking in the Bearing Failure of Composite Laminates," *Compos. Struct.*, 141:184–193.
[20] Schultheisz, C. R. and A. M. Waas. 1996. "Compressive Failure of Composites, Part I: Testing and Micromechanical Theories," *Prog. Aerosp. Sci.*, 32(1):1–42.
[21] Argon, A. S. 1972 "Fracture of Composites," *Treatise Mater. Sci. Technol.*, 1:79–114.
[22] Guynn, E. G., O. O. Ochoa, and W. L. Bradley. 1992. "A Parametric Study of Variables That Affect Fiber Microbuckling Initiation in Composite Laminates: Part 1-Analyses," *J. Compos. Mater.*, 26(11):1594–1616.
[23] Budiansky, B. and N. A. Fleck. 1993. "Compressive Failure of Fibre Composites," *J. Mech. Phys. Solids*, 41(1):183–211.
[24] Jelf, P. M. and N. A. Fleck. 1992. "Compression Failure Mechanisms in Unidirectional Composites," *J. Compos. Mater.*, 26(18):2706–2726.
[25] Basu, S., A. M. Waas, and D. R. Ambur. 2006. "Compressive Failure of Fiber Composites Under Multi-Axial Loading," *J. Mech. Phys. Solids*, 54:611–634.
[26] Basu, S., A. M. Waas, and D. R. Ambur. 2006. "A Macroscopic Model for Kink Banding Instabilities in Fiber Composites," *J. Mech. Mater. Struct.*, 1(6):979–1000.

[27] Costa, S., R. Gutkin, and R. Olsson. 2016. "Finite Element Implementation of a Model for Longitudinal Compressive Damage Growth with Friction," presented at the ECCM17 - 17th European Conference on Composite Materials, June 26-30, 2016.
[28] Leone Jr., F. A. 2015. "Deformation Gradient Tensor Decomposition for Representing Matrix Cracks in Fiber-Reinforced Materials," *Compos. Part Appl. Sci. Manuf.*, 76:334–341.
[29] Gutkin, R., S. T. Pinho, P. Robinson, and P. T. Curtis. 2010. "On the Transition from Shear-Driven Fibre Compressive Failure to Fibre Kinking in Notched CFRP Laminates under Longitudinal Compression," *Compos. Sci. Technol.*, 70(8):1223–1231.
[30] Turon, A., P. P. Camanho, J. Costa, and C. G. Dávila. 2006. "A Damage Model for the Simulation of Delamination in Advanced Composites under Variable-Mode Loading," *Mech. Mater.*, 38(11):1072–1089.
[31] Jones, R. M. 1999. *Mechanics of Composite Materials*. NY: Taylor & Francis Group.
[32] Ramberg W. and W. R. Osgood. 1943. "Description of Stress–Strain Curves by Three Parameters," Technical Note No. 902, National Advisory Committee for Aeronautics.
[33] Puck, A. and H. Schürmann. 1998. "Failure Analysis of FRP Laminates by Means of Physically Based Phenomenological Models," *Compos. Sci. Technol.*, 58(7):1045–1067.
[34] Alfano, G. and E. Sacco. 2006. "Combining Interface Damage and Friction in a Cohesive-Zone Model," *Int. J. Numer. Methods Eng.*, 68(5):542–582.
[35] *ABAQUS Online Documentation: Version 2016*. Providence, RI: Dassault Systèmes Simulia Corporation.
[36] Camanho, P. P., P. Maimí, and C. G. Dávila. 2007. "Prediction of Size Effects in Notched Laminates using Continuum Damage Mechanics," *Compos. Sci. Technol.*, 67(13):2715–2727.
[37] Rose, C. A., C. G. Dávila, and F. A. Leone. 2013. "Analysis Methods for Progressive Damage of Composite Structures," NASA/TM–2013-218024, NASA Langley Research Center.
[38] *HexPly® 8552 Epoxy Matrix Product Data*. Hexcel, Feb., 2014.